Chinese Chemical Letters 33 (2022) 3835–3841

Contents lists available at ScienceDirect

Chinese Chemical Letters

journal homepage: www.elsevier.com/locate/cclet

Microwave-assisted synthesis of oxygen vacancy associated TiO_2 for efficient photocatalytic nitrate reduction

Qian Li[a,1], Yunni Liu[b,1], Zhe Wan[a], Haiyan Cao[a], Shao Zhang[a], Yue Zhou[a], Xingyu Ye[a], Xiaoyan Liu[a,*], Dieqing Zhang[a,*]

[a] The Education Ministry Key Lab of Resource Chemistry, Joint International Research Laboratory of Resource Chemistry, Ministry of Education, and Shanghai Key Laboratory of Rare Earth Functional Materials, College of Chemistry and Materials Science, Shanghai Normal University, Shanghai 200234, China
[b] School of Environmental and Geographical Sciences, Shanghai Normal University, Shanghai 200234, China

ARTICLE INFO

Article history:
Received 27 September 2021
Revised 6 November 2021
Accepted 11 December 2021
Available online 17 December 2021

Keywords:
Photocatalysis
TiO_2
Oxygen vacancy
Nitrate reduction

ABSTRACT

The solar-driven photocatalytic technology has shown great potential in nitrate (NO_3^-) pollutants reduction, however, it has been greatly hindered by the complex preparation and high cost of photocatalysts. Herein, a relatively low-cost photocatalyst, rutile and anatase mixed phase TiO_2 was synthesized by a facile microwave-hydrothermal method. Meanwhile, oxygen vacancy is successfully generated, leading to an acidic surface for strong adsorption towards NO_3^-, which further improved the reduction activity. Compared with the commercial P25, a higher NO_3^- conversion of *ca.* 100% and nitrogen (N_2) selectivity of 87% were achieved under UV (365 nm) irradiation within 2 h. This research provides a promising strategy for designing efficient noble metal free photocatalyst in the NO_3^- reduction.

Nitrogen (N) is an essential nutrient, but when its concentration accumulated to some threshold value, it could be a source of pollution in water or the atmosphere [1]. Nitrates (NO_3^-) as one of the most common N species contaminants in the world, was mainly resulting from the use of nitrogen fertilizers and the dung from large animal farms [2]. However, high intake of nitrate would appear a serious threat to human health, such as an increased risk of natural preterm birth and central nervous system cancers (CNC) in children [2–4]. Furthermore, the nitrate can be reduced to dangerous chemicals, including nitrite (NO_2^-), which caused blue baby syndrome [5]. Thus, many strategies such as reverse osmosis, electrodialysis and ion exchange have been widely studied for removing nitrate from ground water [6]. However, these works highly concentrated on the nitrate conversion into brines instead of removing it to harmless nitrogen (N_2) [7,8].

Photocatalysis as an environment-friendly technology shows great potentials in pollutant removal by directly using solar energy [9–13]. As a semiconductor, titanium dioxide (TiO_2) has been widely used in photocatalytic nitrogen oxides (NO_x) oxidation [10,11,14-17], carbon dioxide (CO_2) reduction [18], hydrogen (H_2) production [19] and removal of volatile organic pollutants (VOCs), *etc.* [20], due to its low-cost, nontoxicity and good stability [21,22]. However, its application in NO_3^- conversion has been limited because of the low efficiency of traditional TiO_2. Noble metals (*e.g.*, Pd, Au, and Ag) loaded TiO_2 have been developed for promoted denitrification performance (Table S1 in Supporting information). However, this noble metal involving strategy greatly increased the cost, which is not practical for large-scale application [8,23,24]. TiO_2 with oxygen vacancies has attracted intensive attention in photocatalytic NO_x removal, H_2 evolution and CO_2 reduction [25–27] owing to the improved charge separation and reactant molecules adsorption. TiO_2 materials with oxygen vacancies are traditionally produced by hydrogen reduction or $NaBH_4$ reduction, both of which are time and energy consuming [28].

Herein, the mixed anatase and rutile phase TiO_2 (TiO_2-A-R) with oxygen vacancies and proper acid sites was successfully prepared by a simple microwave hydrothermal method. The obtained TiO_2-A-R showed outstanding photocatalytic NO_3^- conversion of *ca.* 100% and high N_2 selectivity of 89% under ultraviolet irradiation. This study will provide a novel approach for efficient and low-cost nitrate removal from water.

The synthetic procedure of TiO_2-A-R was illustrated in Scheme 1. In a typical process, potassium titanium oxide oxalate dihydrate and sodium chloride were dispersed in the mixed solution of ethanol and water, keeping stirring for 15 min. Then the as-prepared solution was transferred to the microwave reaction chamber for further microwave treatment under 200 °C for 30 min.

* Corresponding authors.
E-mail addresses: xyliu@shnu.edu.cn (X. Liu), dqzhang@shnu.edu.cn (D. Zhang).
[1] These authors contributed equally to this work.

https://doi.org/10.1016/j.cclet.2021.12.025
1001-8417/

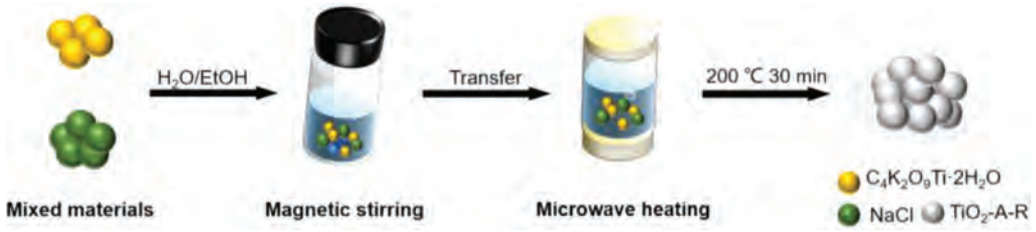

Scheme 1. Schematic illustration of the synthesis processes of TiO_2-A-R.

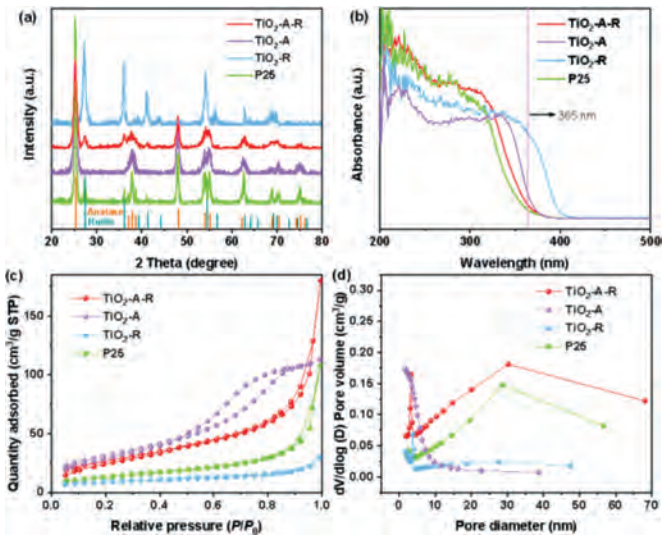

Fig. 1. (a) The XRD pattern, (b) UV–vis DRS spectra, (c) N_2 adsorption-desorption isotherms and (d) pore size distributions of TiO_2-A-R, TiO_2-A, TiO_2-R and P25 samples.

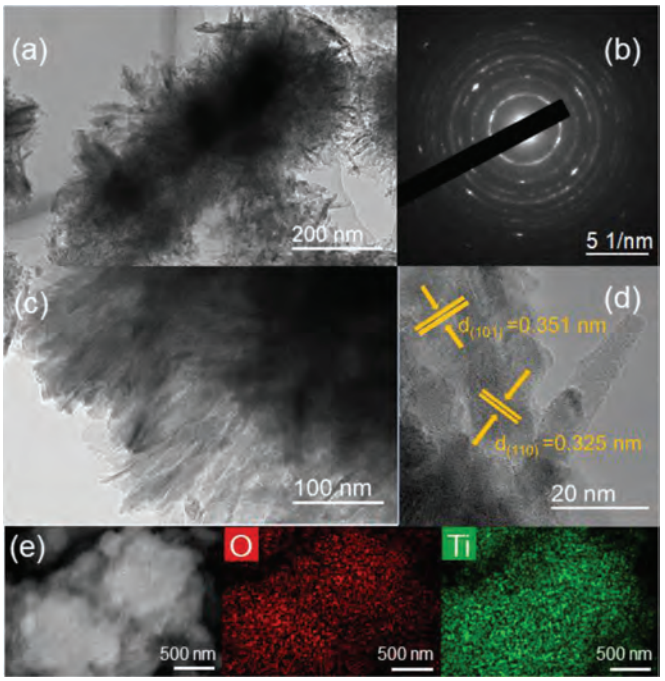

Fig. 2. (a, b) TEM images, (c) SAED pattern, (d) HRTEM image, (e) SEM image and corresponding elemental mappings of TiO_2-A-R sample.

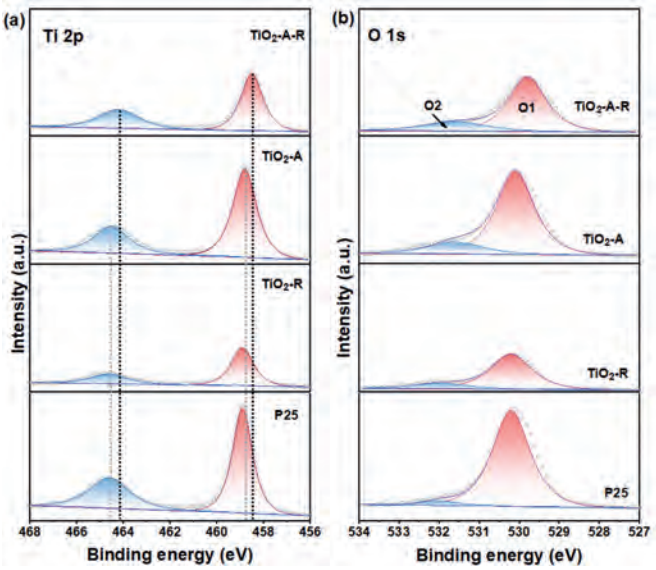

Fig. 3. XPS spectra of (a) Ti 2p and (b) O 1s over TiO_2-A-R, TiO_2-A, TiO_2-R and P25 samples.

As comparison, pure rutile (TiO_2-R) and pure anatase (TiO_2-A) were prepared. As shown in Fig. 1a, the TiO_2-A-R shows the typical X-ray diffraction (XRD) peaks of rutile and anatase phases, which are similar to the commercial P25. Besides, according to the peak intensity, the weight fraction of the rutile in TiO_2-A-R, W_R can be calculated from the formula (Eq. 1) [29,30]. And the weight fraction of the anatase in TiO_2-A-R, W_A can be calculated from the formula as follows (Eq. 2) [31]:

$$W_R = 1/[1 + 0.884\,(A_{ana}/A_{rut})] \quad (1)$$

$$W_A = 1 - W_R \quad (2)$$

In formula, A_{ana} and A_{rut} represented the diffraction peaks intensity of anatase (101) and rutile (110), respectively. Based on the XRD results, the anatase content of TiO_2-A-R was estimated to be 84 wt%. The ultraviolet-visible diffuse reflectance spectra (UV–vis DRS) in Fig. 1b demonstrated that all samples exhibited spectral absorption at 365 nm, which ensured the photocatalyst could be effectively excited under 365 nm irradiation. In addition, based on the UV–vis results, the band gap energy (E_g) of the TiO_2-A-R was calculated as followed (Eq. 3):

$$\alpha h\nu = A(h\nu - E_g)^{n/2} \quad (3)$$

where α, h, ν, A and E_g represented the absorption coefficient, the Planck constant, the light frequency, the constant and band gap, respectively [32]. Furthermore, n was equal to 1/2 or 2 for an indirect or direct band gap semiconductors, respectively. Thus, the estimated E_g of TiO_2-A-R is 3.18 eV (Fig. S1 in Supporting information). The calculated flat band potential (E_{FB}) value of TiO_2-A-R as shown in Fig. S2 (Supporting information) was –0.95 V *vs.* SCE, which is

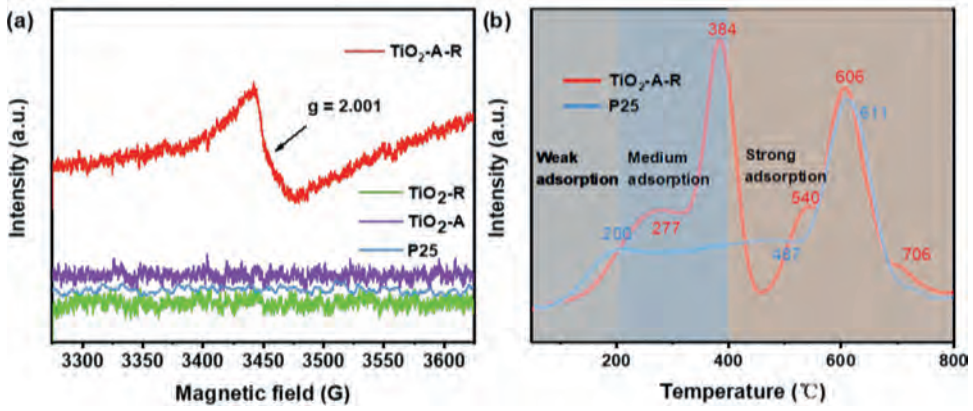

Fig. 4. (a) EPR spectra of TiO_2-A-R, TiO_2-R, TiO_2-A and P25 samples. (b) NH_3-TPD analysis over TiO_2-A-R and P25 sample.

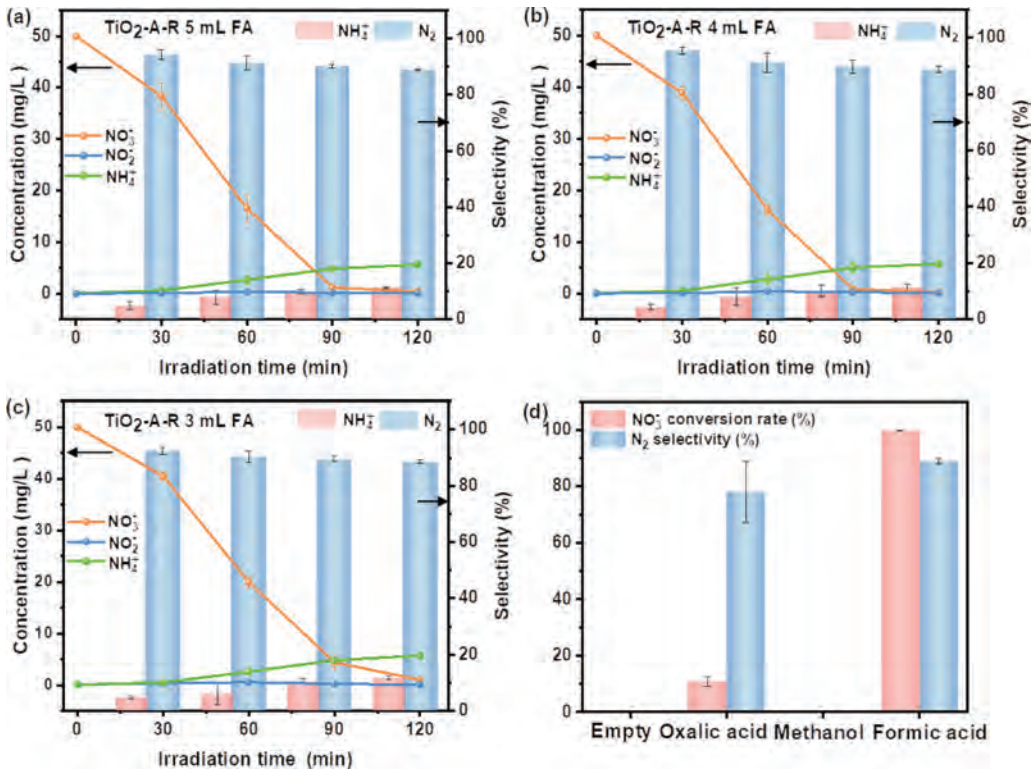

Fig. 5. Photocatalytic nitrate reduction activity of TiO_2-A-R (a-c) with 3–5 mL formic acid and (d) with different hole scavengers.

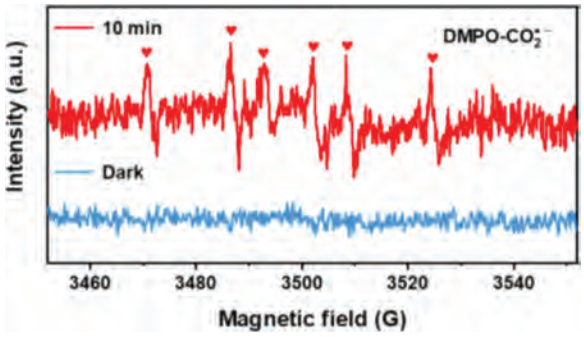

Fig. 6. DMPO spin-trapping EPR spectra of TiO_2-A-R.

corresponding to −0.29 V *vs.* NHE. Besides, TiO_2-A-R as an n-type semiconductor, the conduction band (E_{CB}) was 0.2 V below E_{FB} [33]. Thus, E_{CB} level of TiO_2-A-R was −0.49 eV. And the valence band (VB) was 2.69 eV, which was obtained according to the formula Eq. 4 [32,34]:

$$E_{VB} = E_{CB} + E_g \quad (4)$$

The nitrogen adsorption-desorption isotherms and pore size distributions were displayed in Figs. 1c and d. All the samples showed typical IV isotherms and a pore size distribution ranging from 2 nm to 50 nm, indicating the mesoporous structures. The detailed surfaces areas, pore size and pore volume were listed in Table 1. Compared with other photocatalysts [35–37], TiO_2-A-R had the distinguishing features of larger Brunauer-Emmett-Teller (BET) surface area (97.6 m^2/g), the greater pore volume (0.3 cm^3/g) and the pore diameter (11.4 nm), which might significantly enhance its adsorption ability of reactants and therefore facilitate the targeted reaction [38].

TEM images in Figs. 2a and b suggested that TiO_2-A-R was composed of flaky petal-like structure. Moreover, obvious diffraction rings could be observed in Fig. 2c (the selected area electron

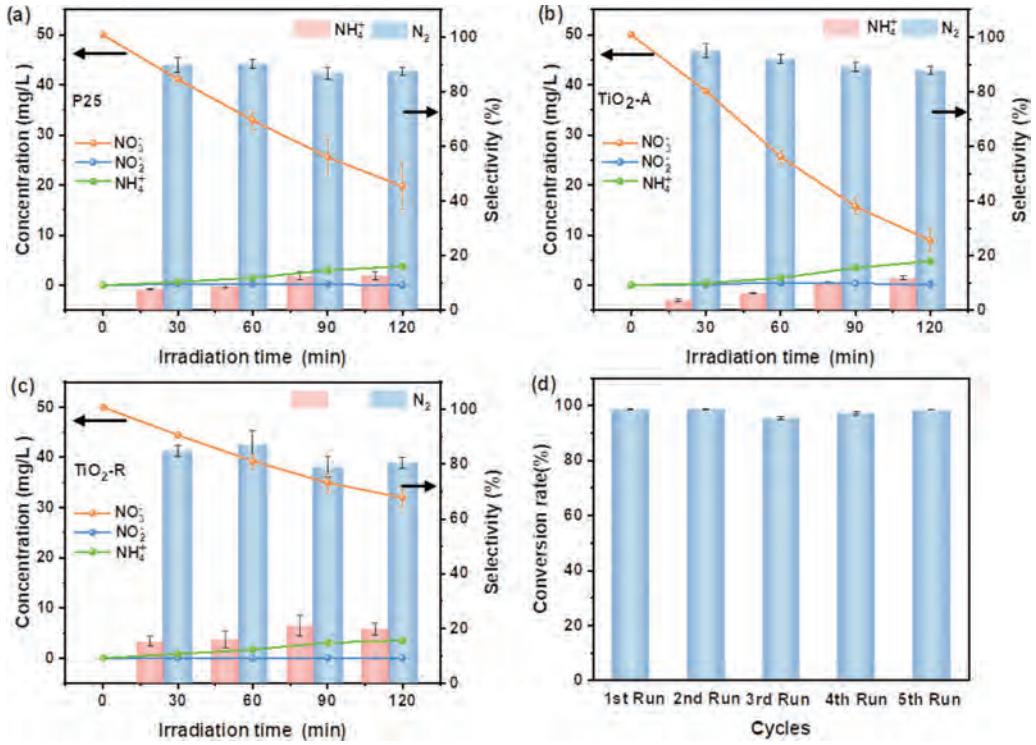

Fig. 7. Photocatalytic nitrate reduction activity of (a) P25, (b) TiO_2-A, and (c) TiO_2-R samples. (d) Cycling stability test of TiO_2-A-R.

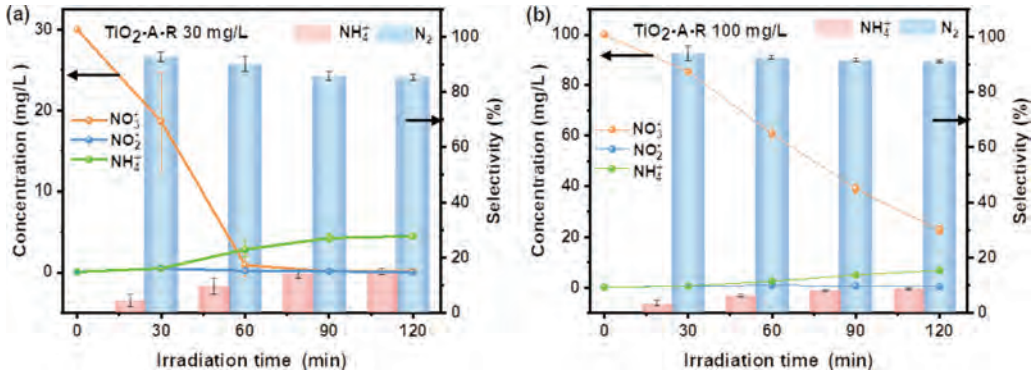

Fig. 8. Photocatalytic nitrate reduction activity over the TiO_2-A-R sample involving different NO_3^- initial concentrations of (a) 30 and (b) 100 mg/L.

Table 1
BET properties of TiO_2-A-R, TiO_2-A, TiO_2-R and P25 photocatalysts.

Sample	S_{BET} (m^2/g)	D_p (nm)	V_P (cm^3/g)
TiO_2-A-R	97.6	11.4	0.3
TiO_2-A	113.0	5.0	0.2
TiO_2-R	30.9	5.9	0.1
P25	48.6	13.7	0.2

diffraction, SAED), indicating the TiO_2-A-R had good crystallinity [39]. Meanwhile, the lattice spacing of 0.351 nm and 0.325 nm were also clearly detected in Fig. 2d, which corresponded to (101) and (110) plane of anatase and rutile, respectively [40]. The element mappings demonstrated the homogeneous distribution of Ti and O in TiO_2-A-R (Fig. 2e). These results further confirmed the successful synthesis of mixed-phase titanium dioxide.

In order to probe the surface chemical compositions and the binding configuration of all the samples, X-ray photoelectron spectroscopy (XPS) measurement was performed. P25 and TiO_2-R show the peaks located at 458.9 and 464.6 eV corresponding to Ti $2p_{3/2}$ and Ti $2p_{1/2}$ (Fig. 3a). These peaks of TiO_2-A slightly shifted to lower binding energies. Notably, a clearly negative shift was also observed in the TiO_2-A-R, indicating the existence of Ti^{3+} [41]. Meanwhile, the O 1s XPS spectra of TiO_2-A-R presented two peaks centered at ~529.8 and ~531.6 eV (Fig. 3b), representing for the lattice oxygen and oxygen vacancy, respectively [7]. And the area ratio of oxygen vacancy peak (named O2) to the sum area of the O1 and O2 peaks (named Os) is shown in Table S2 (Supporting information). The O2/Os of TiO_2-A-R had the largest percentage (22.7%), which demonstrated that oxygen vacancy rooted more in the TiO_2-A-R sample [28].

Moreover, the strong electron paramagnetic resonance (EPR) signal (Fig. 4a) in TiO_2-A-R with a g-value of 2.001 further verified the existence of oxygen vacancy [42], which might play a vital role in promoting the rapid conversion of nitrate as previously reported [28]. Furthermore, the catalysts' activities are closely related to their surface properties such as alkaline and acidity properties [43]. Moreover, the NO_3^- presents Lewis base due to its electronegativity, which implies that it is easier to combine with the Lewis acid catalyst surface [44,45]. Thus temperature-programmed

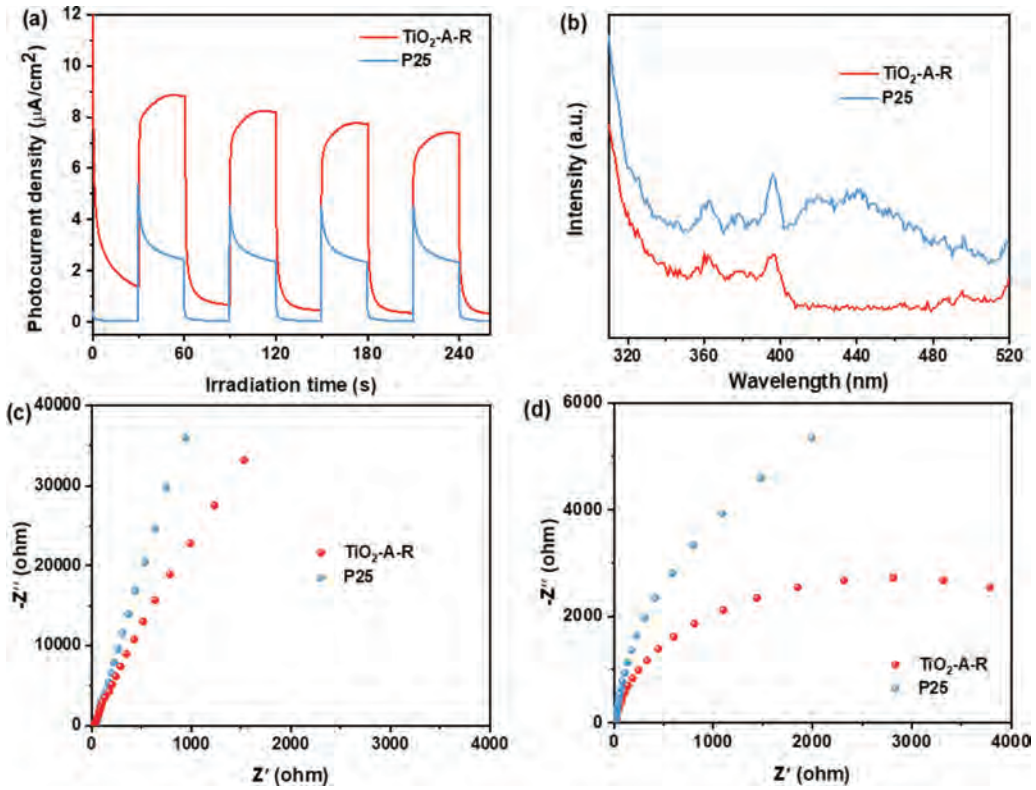

Fig. 9. (a) Photocurrent density, (b) PL spectra ($e_x = 290$ nm), electrochemical impedance spectra (c) in dark and (d) light irradiation of TiO_2-A-R and P25 samples.

desorption of ammonia (NH_3-TPD) of P25 and TiO_2-A-R were performed from 50 °C to 800 °C to find out their surface properties, and the curves were illustrated in Fig. 4b [46,47]. The desorption peaks of NH_3 located below 200 °C, 200–400 °C and above 400 °C are considered as indicators of the weak, medium and strong acid sites, respectively [48]. P25 exhibited three NH_3 desorption peaks at 200, 487 and 611 °C, respectively. The former one is assigned to the weak acid sites and the other two peaks are indexed to the strong acid sites. As comparison, there are only medium (suggested by the peaks at 277 and 384 °C) and strong acid sites (suggested by the peaks at 540, 606 and 706 °C) observed, demonstrating its more acidic surface. As displayed in Table S3 (Supporting information), TiO_2-A-R shows a larger peak area than that of P25, confirming there are more active sites to possibly absorb and reduce the NO_3^- [44,49].

Normally, NO_3^- could be reduced to N_2, NO_2^- and ammonium (NH_4^+), but both NO_2^- and NH_4^+ are hazardous to the environment. An ideal photocatalyst should have high NO_3^- conversion and good N_2 selectivity [24,50]. In order to inhibit the rapid recombination of electron-hole pairs, formic acid (FA) was selected as a hole scavenger in this reaction [51]. To exclude the catalytic effect of FA on NO_3^- reduction, we conducted a control experiment (in FA without photocatalyst added) and the results were shown in Fig. S3a (Supporting information). No catalytic activity was observed in the absence of the photocatalyst, and thus we can conclude that FA itself will not react with NO_3^- and promote NO_3^- reduction. Then, TiO_2-A-R (0.060 g) and various amounts of FA were dispersed into 60 mL nitrate solution (50 mg/L) to evaluate the optimal photocatalytic performance. As shown in Figs. 5a-c, the activity sequence involving different amounts of FA were summarized as 5 mL FA ≈ 4 mL FA > 3 mL FA. Meanwhile, almost no NO_2^- was detected in the reaction process of the three controlled trials. When the reaction progressed to 120 min, the average conversion of NO_3^- involving 3 mL FA was 98%, the average selectivity of N_2 and NH_4^+ were 88% and 12%, respectively. The experiments with 4 mL or 5 mL FA showed similar nitrate conversion (almost 100%), N_2 selectivity (89%) and NH_4^+ selectivity (11%). Therefore, we determined adding 4 mL FA as the optimal hole scavenger amount for this reaction.

According to the literature, different hole scavengers such as oxalic acid (OC) and methanol may also be favorable for the photocatalytic nitrate reduction [50]. Thus, the 4 mL 0.1 mol/L methanol and OC solution was introduced for photocatalytic NO_3^- (50 mg/L) reduction experiment as shown in Fig. 5d. The OC involving system demonstrated the NO_3^- conversion of 11% and the 78% N_2 selectivity, which were much lower than that of FA. No NO_3^- conversions were observed in methanol involving system or hole scavengers absence system, indicating that FA significantly improved the photocatalytic activity [24]. Based on the previous study [51], we confirm that carbon dioxide anion radical ($CO_2^{\bullet-}$) generated by reacting FA with photogenerated holes of photocatalyst has strong reductive ability for NO_3^- conversion to N_2. Then, EPR test was carried out to probe the production of $CO_2^{\bullet-}$ in the TiO_2-A-R system. As shown in Fig. 6, no signals were detected under dark conditions. While under light irradiation, a six-line DMPO-$CO_2^{\bullet-}$ spin adduct signal was formed with hyperfine parameter of magnetic factor $g = 2.0059$ (Fig. S3b in Supporting information), which can be assigned to reductive $CO_2^{\bullet-}$ species for further promoting NO_3^- degradation [52–54]. These results clearly indicated the important promoted effect of FA in the photocatalytic NO_3^- reduction reaction using noble-metal free TiO_2 as photocatalysts.

In order to compare the contribution of TiO_2-A-R, the performance of TiO_2-A, TiO_2-R and commercial P25 were evaluated in 4 mL FA and NO_3^- (50 mg/L) mixture solution system (Figs. 7a-c.). The photocatalytic removal rate of these samples followed the order of TiO_2-A-R (100%) > TiO_2-A (82%) > P25 (61%) > TiO_2-R (36%). And the selectivity of N_2 presented the trend of TiO_2-A-R (89%)

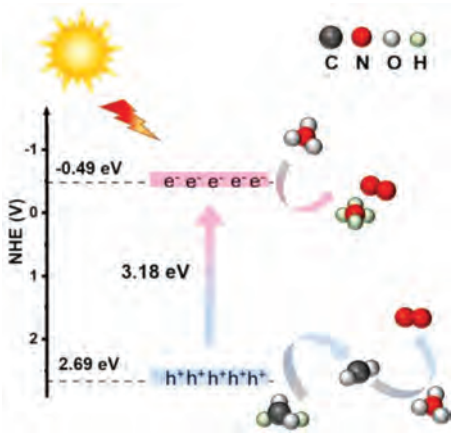

Scheme 2. Schematic illustration of photocatalytic reduction mechanism of NO_3^-.

> TiO_2-A (88%) > P25 (87%) > TiO_2-R (80%). Obviously, TiO_2-A-R showed the enhanced ability of NO_3^- reduction, which may be attributed to the existence of Ov and acid sites [28]. In addition, the cycling durability of TiO_2-A-R was conducted and displayed in Fig. 7d. After five cycles, the photocatalyst still had 98% NO_3^- conversion, demonstrating its great stability and big potential for practical application. Moreover, when the concentration of the initial NO_3^- solution was diluted to 30 mg/L (Fig. 8a), the NO_3^- conversion was achieved 100% after 90 min reaction and the selectivity of N_2 and NH_4^+ reached 86% and 14%, respectively. Even when the NO_3^- concentration was increased to 100 mg/L, a high NO_3^- removal of 77% and N_2 selectivity of 91% were achieved after 120 min reaction (Fig. 8b), implying the excellent activity of TiO_2-A-R in a wide NO_3^- concentrations range.

The photocurrent response (Fig. 9a) was carried out to evaluate the charge transport properties [10]. Compared with commercial P25, TiO_2-A-R has a higher photocurrent density, which demonstrates the improved light source usage rate and effective separation of e^- and h^+ excited by photons [55]. In addition, the steady-state photoluminescence (PL) spectrum was measured to investigate the electrons and holes recombination (Fig. 9b). Notably, a lower emission peak of TiO_2-A-R can be obtained, demonstrating the improved charge carrier separation efficiency [56]. And TiO_2-A-R showed the smaller radius under dark and 365 nm UV-LED irradiation (Figs. 9c and d), indicating a better conductivity [9]. These factors co-contributed the excellent NO_3^- conversion and good N_2 selectivity.

Based on the above discussion, the possible NO_3^- degradation mechanism is proposed as shown in Scheme 2. Firstly, TiO_2-A-R is excited to produce photo-generated electron-hole pairs under the UV-LED irradiation (Eq. 5). Then the electrons are consumed by NO_3^- to generate N_2 or NH_4^+ (Eqs. 6 and 7) [24]. Meanwhile, the photo-generated holes are scavenged by FA to produce $CO_2^{\bullet-}$ species, which further reduces NO_3^- to N_2 (Eqs. 8 and 9) [8,44,57-59].

$$TiO_2 + h\nu \rightarrow e^- + h^+ \quad (5)$$

$$NO_3^- + 6H^+ + 5e^- \rightarrow 1/2N_2 + 3H_2O \quad (6)$$

$$NO_3^- + 10H^+ + 8e^- \rightarrow NH_4^+ + 3H_2O \quad (7)$$

$$HCOO^- + h^+ \rightarrow CO_2^{\bullet-} + H^+ \quad (8)$$

$$NO_3^- + 5CO_2^{\bullet-} + 6H^+ \rightarrow 1/2N_2 + 5CO_2 + 3H_2O \quad (9)$$

In conclusion, the mixed TiO_2 photocatalyst with oxygen vacancy was successfully synthesized *via* a facile microwave-assisted method. It has a NO_3^- conversion up to *ca.* 100% under 2 h ultraviolet radiation, which is much high than that of commercial P25 (61%). Moreover, the N_2 selectivity is as high as 89%. This work provides a novel strategy to design noble metal free photocatalysts for cheap, safe and efficient nitrate removal.

Declaration of competing interest

The authors declare no competing financial interest.

Acknowledgments

This work was supported by the National Key Research and Development Program of China (No. 2020YFA0211004), and National Natural Science Foundation of China (Nos. 21876112, 21876113, 22022608, 92034301), "111" Innovation and Talent Recruitment Base on Photochemical and Energy Materials (No. D18020), Ministry of Education, and Shanghai Key Laboratory of Rare Earth Functional Materials, Shanghai Engineering Research Center of Green Energy Chemical Engineering (Nos. 18DZ2254200) and Shanghai government (Nos. 18SG41, 309-AC9103–21–413002, 19YF1436600).

Supplementary materials

Supplementary material associated with this article can be found, in the online version, at doi:10.1016/j.cclet.2021.12.025.

References

[1] H. Shibata, R. Ban, N. Hirano, et al., Environ. Pollut. 288 (2021) 117695–117705.
[2] L.T. Stayner, J. Schullehner, B.D. Semark, et al., Environ. Int. 155 (2021) 106613–106621.
[3] A.R. Sherris, M. Baiocchi, S. Fendorf, et al., Environ. Health Perspect. 129 (2021) 57001–57011.
[4] Y.J. Shih, Z.L. Wu, Appl. Catal. B: Environ. 285 (2021) 119784–119793.
[5] X. Huo, D.J. Van Hoomissen, J. Liu, S. Vyas, T.J. Strathmann, Appl. Catal. B: Environ. 211 (2017) 188–198.
[6] F. Ni, Y. Ma, J. Chen, W. Luo, J. Yang, Chin. Chem. Lett. 32 (2021) 2073–2078.
[7] R. Jia, Y. Wang, C. Wang, et al., ACS Catal. 10 (2020) 3533–3540.
[8] T. Caswell, M.W. Dlamini, P.J. Miedziak, et al., Catal. Sci. Technol. 10 (2020) 2082–2091.
[9] X. Chen, Y. Cai, R. Liang, et al., Appl. Catal. B: Environ. 267 (2020) 118687–118694.
[10] S. Xiao, D. Zhang, D. Pan, et al., Nat. Commun. 10 (2019) 1570–1579.
[11] S. Xiao, Z. Wan, J. Zhou, et al., Environ. Sci. Technol. 53 (2019) 7145–7154.
[12] X. Chen, S. Xiao, H. Wang, et al., Angew. Chem. Int. Ed. 59 (2020) 17182–17186.
[13] A.U.R. Bacha, I. Nabi, Z. Fu, et al., Chin. Chem. Lett. 30 (2019) 2225–2230.
[14] W. Dai, Y. Tao, H. Zou, et al., Environ. Sci. Technol. 54 (2020) 5902–5912.
[15] M.C. Wen, S.S. Zhang, W.R. Dai, G.S. Li, D.Q. Zhang, Chin. J. Catal. 36 (2015) 2095–2102.
[16] W. Zhu, S. Xiao, D. Zhang, et al., Langmuir 31 (2015) 10822–10830.
[17] D. Zhang, G. Li, F. Wang, J.C. Yu, CrystEngComm 12 (2010) 1759–1763.
[18] S. Zhu, X. Chen, Z. Li, et al., Appl. Catal. B: Environ. 264 (2020) 118515–118524.
[19] Y. Ma, X. Wang, C. Li, Chin. J. Catal. 36 (2015) 1519–1527.
[20] J. Deng, S. Xiao, B. Wang, et al., ACS Appl. Mater. Interfaces 12 (2020) 51537–51545.
[21] G. Li, D. Zhang, J.C. Yu, M.K. Leung, Environ. Sci. Technol. 44 (2010) 4276–4281.
[22] Y. Jiang, Y. Qin, T. Yu, S. Lin, Chin. Chem. Lett. 32 (2021) 1823–1826.
[23] J.A. Anderson, Catal. Today 175 (2011) 316–321.
[24] Z. Hou, F. Chen, J. Wang, C.P. François-Xavier, T. Wintgens, Appl. Catal. B: Environ. 232 (2018) 124–134.
[25] H. Shang, M. Li, H. Li, et al., Environ. Sci. Technol. 53 (2019) 6444–6453.
[26] T. Wang, X. Tao, X. Li, et al., Small 17 (2021) 2006255–2006264.
[27] J. Li, M. Zhang, Z. Guan, et al., Appl. Catal. B: Environ. 206 (2017) 300–307.
[28] C. Wang, S. Dong, Y. Wang, et al., Chem. Eng. J. 397 (2020) 125435–125444.
[29] J. Zhang, M.J. Li, Z.C. Feng, J. Chen, C. Li, J. Phys. Chem. B 110 (2006) 927–935.
[30] S. Shen, X. Wang, T. Chen, Z. Feng, C. Li, J. Phys. Chem. C 118 (2014) 12661–12668.
[31] H. Li, X. Shen, Y. Liu, et al., Alloys Compd. 646 (2015) 380–386.
[32] H. Wang, R. Zhao, H. Hu, et al., ACS Appl. Mater. Interfaces 12 (2020) 40176–40185.
[33] X. He, M. Wu, Z. Ao, et al., J. Hazard. Mater. 403 (2021) 124048–124056.
[34] X. Xu, S.N. Xiao, H.J. Willy, et al., Appl. Catal. B: Environ. 262 (2020) 118307–118315.
[35] J.J. Li, S.C. Cai, Z. Xu, et al., J. Hazard. Mater. 325 (2017) 261–270.
[36] Z.Y. Wu, M. Karamad, X. Yong, et al., Nat. Commun. 12 (2021) 2870–2879.

[37] G. Fan, J. Zhan, J. Luo, et al., J. Hazard. Mater. 404 (2021) 124062–124079.
[38] X. Zeng, X. Sun, Y. Yu, H. Wang, Y. Wang, Chem. Eng. J. 378 (2019) 122226–122235.
[39] X. Zhang, G. Li, Y. Zhang, et al., Nano Energy 86 (2021) 106094–106103.
[40] G. Cheng, X. Liu, X. Song, et al., Appl. Catal. B: Environ. 277 (2020) 119196–119212.
[41] M. He, J. Ji, B. Liu, H. Huang, Appl. Surf. Sci. 473 (2019) 934–942.
[42] X. Song, W. Li, X. Liu, et al., J. Energy Chem. 55 (2021) 154–161.
[43] S. Tian, Y. Wu, H. Ren, et al., Fuel Process. Technol. 193 (2019) 53–62.
[44] X. Li, S. Wang, H. An, et al., Appl. Surf. Sci. 539 (2021) 148257–148266.
[45] J. You, W. Sun, S. Su, et al., Chem. Eng. J. 400 (2020) 125915–125928.
[46] S. Ali, L. Chen, Z. Li, et al., Appl. Catal. B: Environ. 236 (2018) 25–35.
[47] M.S. Maqbool, A.K. Pullur, H.P. Ha, Appl. Catal. B: Environ. 152-153 (2014) 28–37.
[48] W. Zhu, X. Tang, F. Gao, et al., Chem. Eng. J. 385 (2020) 123797–123806.
[49] S. Ali, L. Chen, F. Yuan, et al., Appl. Catal. B: Environ. 210 (2017) 223–234.
[50] S. Challagulla, K. Tarafder, R. Ganesan, S. Roy, J. Phys. Chem. C 121 (2017) 27406–27416.
[51] H.O. Tugaoen, S. Garcia-Segura, K. Hristovski, P. Westerhoff, Sci. Total Environ. 599-600 (2017) 1524–1551.
[52] N. Tong, Y. Wang, Y. Liu, et al., J. Catal. 361 (2018) 303–312.
[53] J. Chen, J. Liu, J. Zhou, D. Chen, J. Water Process. Eng. 33 (2020) 101097–101104.
[54] X. Liu, J. Zhong, L. Fang, et al., Chem. Eng. J. 303 (2016) 56–63.
[55] D. Pan, S. Xiao, X. Chen, et al., Environ. Sci. Technol. 53 (2019) 3697–3706.
[56] Y. Geng, D. Chen, N. Li, et al., Appl. Catal. B: Environ. 280 (2021) 119409–119417.
[57] H.T. Ren, S.Y. Jia, J.J. Zou, S.H. Wu, X. Han, Appl. Catal. B: Environ. 176-177 (2015) 53–61.
[58] J. Sá, C.A. Agüera, S. Gross, J.A. Anderson, Appl. Catal. B: Environ. 85 (2009) 192–200.
[59] Y.A. Shaban, A.A. El Maradny, R.K. Al Farawati, J. Photochem. Photobiol. A 328 (2016) 114–121.